Mise en place de l'extraction liquide-liquide en microsystèmes établir des écoulements segmentés à façon pour optimiser le transfert de masse

A. Vansteene, J.-P. Jasmin, L. Al Ahmad, S. Cavadias, G. Cote, C. Mariet

Liquid-liquid extraction in microsystems: establish segmented flows to optimize mass transfer

A. VANSTEENE[a], J.-P. JASMIN[a], L. AL AMHAD[b], S.CAVADIAS[b,c], G. COTE[b], C. MARIET[a]

a. Den - Service d'Etudes Analytiques et de Réactivité des Surfaces (SEARS), CEA, Université Paris-Saclay, F-91191, Gif sur Yvette, France, axel.vansteene@cea.fr
b. PSL Research University, Chimie ParisTech - CNRS, Institut de Recherche de Chimie Paris, 75005, Paris, France
c. UPMC – Univ Paris 06, 4 Place Jussieu, 75005 Paris, France

Résumé :

L'extraction liquide-liquide est couramment utilisée pour les analyses radiochimiques. Miniaturisée, elle peut bénéficier des avantages des outils microfluidiques qui sont la possibilité de réaliser des couplages, le contrôle précis de l'aire interfaciale entre les phases aqueuse et organique en présence, et des temps de contact. Une première étude, dédiée à l'extraction liquide-liquide en flux parallèles d'europium en milieu nitrique par le N,N'-dimethyl N,N'-dibutyl tetradecylmalonamide [1, 2], a permis de mettre en évidence les limitations des flux parallèles pour un système chimique lent. Une façon d'optimiser les rendements d'extraction des systèmes cinétiquement lents est de mettre en œuvre des écoulements permettant d'augmenter l'aire interfaciale spécifique. C'est pourquoi nous étudions la formation d'écoulements segmentés à façon en fonction des propriétés physico-chimiques d'un système chimique biphasique, des débits et des dimensions d'une jonction en flux focalisé. L'utilisation de deux modèles de calcul des tailles de gouttes en régimes d'écoulements transitoire et d'égouttement a été validée et servira de base à l'optimisation de l'aire interfaciale spécifique.

Abstract :

Liquid-liquid extraction is commonly used for radiochemical analysis. When miniaturized, it can benefit from the advantages of microfluidic tools i.e. possible coupling, precise control of the interfacial area between the aqueous and organic phases, and contact time. A first study, dedicated to liquid-liquid extraction with parallel flows of europium diluted in nitric acid by the N,N'-dimethyl-N,N'-dibutyltetradecylmalonic diamide [1, 2], allowed us to highlight the limitations of parallel flows for a slow chemical system. One way to optimize yields of extraction of the kinetically slow systems is to increase the specific interfacial area. For this reason, segmented flows formation and characteristics were investigated, as a function of the physicochemical properties of a biphasic system, flow rates and the dimensions of a focalized flux junction. In the following, two multiphase models of the droplets size corresponding to the transition and dripping regimes were validated and will be used for the optimization of the specific interfacial area.

Mots clefs : Lab-on-Chip –Radiochemical Analysis – Microfluidics – Hydrodynamics – Comsol Multiphysics® - Modeling

1 Introduction

The analysis of radionuclides present in the fuel, or medium or high activity waste, depends on operating protocols including a given sequence of steps dedicated to the isolation of the radionuclides of interest from the interfering ones. Liquid-liquid extraction (LLE) is commonly implemented in glove boxes or shielded enclosures [3], generates large amounts of waste and cannot be easily automated. One way to solve these problems is to miniaturize the chemical operation. Microdevices can reduce the consumption of radioactive samples and the production of solid and liquid waste at the end of the analytical procedure [4]. From the radiation protection point of view, the reduction of the volume of the samples by a 1000-factor, for example, would lead to a quasi-proportional decrease in the activity manipulated by the experimenter and therefore enable the user to consider the use of least restrictive protection devices: from a glovebox to a ventilated hood for instance [5]. From the analytical point of view, microsystems have the advantage of reducing the overall analysis time thanks to short diffusion lengths [6, 7], parallelization, automation [8] and increased specific interfacial area (area/volume ratio) [9].
LLE is based on the difference of affinity of a solute towards two immiscible phases. A feeding aqueous solution containing the solutes to separate is put in contact with an organic phase, called solvent, which selectively extract one or more initially present solutes from the aqueous phase [10]. The solvent consists in a selective extractant diluted in a diluent containing or not a phase modifier. In microsystems, the two immiscible phases are put in contact in a microchannel where they circulate in parallel or segmented flows [11] (figure 1). Parallel flows allow to easily retrieve the two phases at the output of microchannel and so facilitate the coupling with other chemistry steps or with detection [12, 13]. However, even if the specific interfacial area in parallel flow is higher than that obtained in macroscopic mixer-decanter, it remains lower than that obtained with segmented flows. Dessimoz et al. [9] estimated the value of the specific interfacial area with parallel flows in a glass microsystem to 6850 m^{-1} and compared it with the value of 11,000 m^{-1} obtained with segmented flows in the same microchannel. An increased specific interfacial area promotes mass transfer. In addition, the segmentation of the flows assists mixture with advective movements. Within a drop flowing in a microchannel, the velocity field is not uniform, and recirculation patterns involve the renewal of reagents at the interface [9, 14 - 20]. As a consequence, mass transfer is greatly enhanced. To improve the mass transfer, one can also consider counter-current flows but this was rarely achieved and in a 4 mm length microchannel [21].

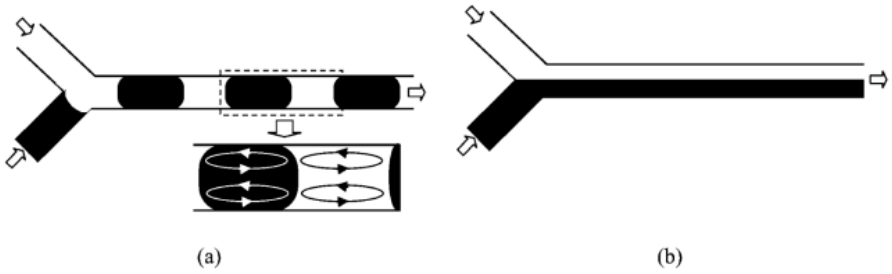

Figure 1 : Diagram of stable flows in a liquid-liquid microchip: (a) segmented flows, (b) parallel flows [22]

Our aim is to increase the specific interfacial area [23-25] in order to optimize mass transfer for liquid-liquid extraction systems known to have slow kinetics, as the organic/ aqueous N,N′-dimethyl-N,N′-

dibutyltetradecylmalonic diamide (DMDBTDMA)-dodecane / Eu(III)-HNO_3 chemical system [26]. In 2001, Ganan-Calvo et al. [27] developed a focalized flux (FF)-junction to form an emulsion of gas in a liquid, which use spread to liquid-liquid segmented flow with Anna et al. [28]. Using a hole allows a better control of drops sizes smaller than the width of the channel, with an often less than 1% polydispersity [29, 30]. By implementing segmented flows using a FF-junction, we were able to create monodisperse segmented flows, optimize droplets characteristics (size, frequency, spacing), and therefore increase the specific interfacial area.

2 Experimental

2.1 Reagents

DMDBTDMA (98.8%) was synthesized by Pharmasynthese SAS and n-dodecane was supplied by Sigma-Aldrich. Organic extractant solutions were prepared by dissolving weighted amounts of the desired compound in the diluent. All aqueous solutions were prepared with 18-MΩ deionized water produced by a Milli-Q water purification system (Millipore, Bedford, MA). Europium nitrate solutions were prepared by dissolving $Eu(NO_3)_3$ granules in pre-equilibrated 4M nitric solutions. Aqueous and organic phases were mutually pre-saturated by contact under shaking overnight.
Solution densities were measured using a DMA 4500 density meter (Anton Paar, Austria). The temperature was set at 298.150 ± 0.001 K. The accuracy of the density measurements was about $\pm 3.10^{-6}$ $kg.dm^{-3}$. Viscosity at atmospheric pressure was measured with a rotational automated viscometer Lovis 2000 M/ME (Anton Paar, Austria) [31]. The accuracy of viscosity measurements was better than 0.5%. Interfacial tensions were measured using the plate method with the tensiometer K100C (Krüss). Experimental values of densities, viscosities and interfacial tension are presented Table 1.

Composition		Density ρ (kg/m^3)	Dynamic viscosity η (mPa.s)	Interfacial tension σ (mN/m)
Continuous aqueous phase	$[HNO_3]$ = 4 M $[Eu(III)] = 10^{-2}$ M	1131.14 ± 0.01	1.186 ± 0.001	29.82 ± 0.41
Dispersed organic phase	[DMDBTDMA] = 1 M in dodecane	846.04 ± 0.01	18.11 ± 0.02	

Table 1 : Physico-chemical properties of the continuous aqueous phase and dispersed organic phase

2.2 Experimental set-up

Figure 2-a is a diagram of the experimental set up. Two peristaltic Mitos P-Pumps (Dolomite, UK) were used to feed the aqueous and organic phases into a focalized flux (FF)-junction glass chip. The aqueous phase was first injected in the in-built T-junction, in order to create two streams of equal velocities, which streams were brought to the main FF-junction where the organic phase was dispersed. A picture of the droplet junction microchip in its holder is provided in Figure 2-b. The droplet junction chip is a hydrophilic glass microfluidic device designed for generating droplets. On the chip, there are two separate droplet junctions, a FF-junction and a T one. In the FF-Junction, the dimension of the wide channel cross-section are depth x width = 100 µm x 300 µm, and the dimensions at the channel cross-section at junction are depth x width= 100 µm x 105 µm. The channel length after junction is 11.25mm. The channel length in which segmented flow occurred comprised two sections, one of which being the

microchannel itself, and the other being a PEEK tubing from the chip to the outlet. In all the cases studied, the organic phase was dispersed in an aqueous continuous phase, which preferentially wets the microchannel walls. After each set of experiments, the microchannel was cleaned with isopropanol to remove any residual organic liquid and then flushed with compressed air.

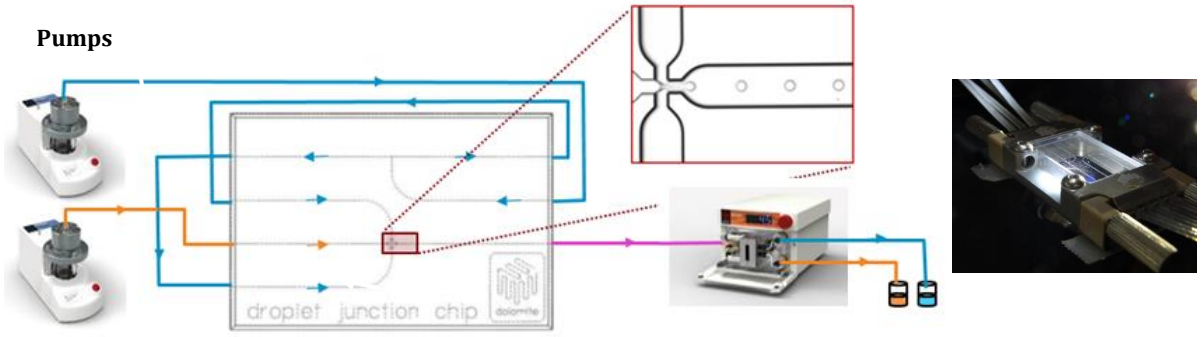

(a) (b)

Figure 2: (a) Experimental set-up used for the production and observation of segmented flows – pumps, house-made pressure chambers, chip, 250 ID high-purity perfluoroalkoxy (HPFA) tubing, blue: the aqueous phase, orange: the organic phase, pink : the segmented flow in which the organic phase is dispersed (b) Picture of the droplet junction chip with both a T- and FF-junctions.

2.3 Droplet morphometry and velocity

A high speed camera (Photron Mini AX-100) was mounted on a digital inverted microscope (DEMIL LED Leica) equipped with an objective lens with a 40 times magnification to image directly the segmented flow in the microchannel with adjustable frame rate, from 2,000 to 10,000 fps depending on droplet velocities (Figure 2-A). The recorded videos were analyzed using a Droplet Morphometry and Velocity (DMV) software [32], which provided droplets volumes, spacing, and velocities (Figure 3).

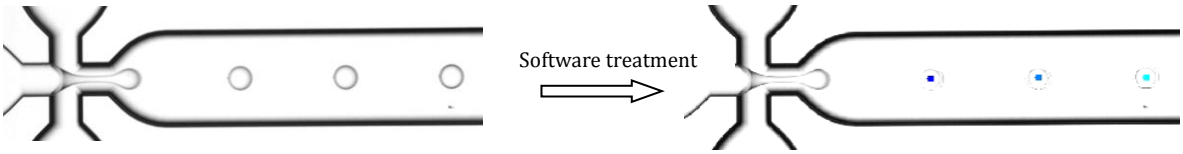

Figure 3: Droplet identification using Droplet Morphometry and Velocimetry Software, Dodecane – [DMDBTDMA]= 1 M droplets in [HNO_3]= 4 M – [Eu(III)]=10^{-2} M, $P_c = 2.280.10^5\ Pa, P_d = 2.180.10^5\ Pa$ and $Q_c = 6.60\ mL.h^{-1}, Q_d = 0.22\ mL.h^{-1}$, [32].

3 Results and discussion

We study which flow regime can be formed in the FF-junction for the biphasic system DMDBTDMA – dodecane / Eu (III) - HNO_3. In particular, we want to understand how flow rates and viscosities of the phases involved in the calculation of capillary numbers affect the hydrodynamics of the system as well as the size of the drops of the dispersed phase.

3.1 Flow regimes models

Hydrodynamic regimes are described in the literature [30 - 36] as a function of capillary numbers of dispersed and continuous phases in FF-junctions. The capillary numbers of the continuous phase Ca_c and of the dispersed phase Ca_d are written with relations (1) and (2), respectively.

$$\mathrm{Ca_c} = \frac{\eta_c}{\sigma}\frac{Q_c}{hw} \quad (1) \qquad \text{and} \qquad \mathrm{Ca_d} = \frac{\eta_d}{\sigma}\frac{Q_d}{hw} \quad (2)$$

With
η_c, η_d the viscosities of the continuous and dispersed phases, respectively (Pa.s).
Q_c, Q_d the flow rates of the continuous and dispersed phases, respectively ($m^3.s^{-1}$).
σ the interfacial tension ($N.m^{-1}$).
w the diameter of the microchannels at the inlet of the continuous and dispersed phases (m).
The subscripts c and d design the continuous and dispersed phases.

Based on capillary numbers, a flow pattern cartography was established as a function of flow rates of the phases by concatenation of the aforementioned results from the literature [30 , 33-36]. Figure 4-a, we observe both capillary numbers have an effect on droplet generation and five hydrodynamic regimes can be seen. For our application, the tubing regime (which is equivalent to an annular regime) is not attractive because it does not allow to vary the specific interfacial area, neither is the jetting regime which is known to be a regime a high polydispersity. In the squeezing regime, the dispersed phase first enters the junction, then obstructs the junction, leading to a growing pressure in the continuous phase inlet, which ends in dispersed phase constriction and droplet creation. The transition regime is located at slightly higher continuous phase flow rates; therefore, the capillary effects must be taken into account. Choosing to work in the transition regime, a compromise between a high enough specific interfacial area and a sufficiently long contact time of the phases is achieved.
Then, in our study, most experimental data belongs to the transition regime between squeezing and dripping (Figure 4-a). As a consequence, transition regime model and an early-dripping model will be considered. As depicted in Figure 4-b, droplet formation characteristics are varying all along the transition regime, from a squeezing-like formation to a dripping-like formation, explaining our need for a comprehensive empirical equation.

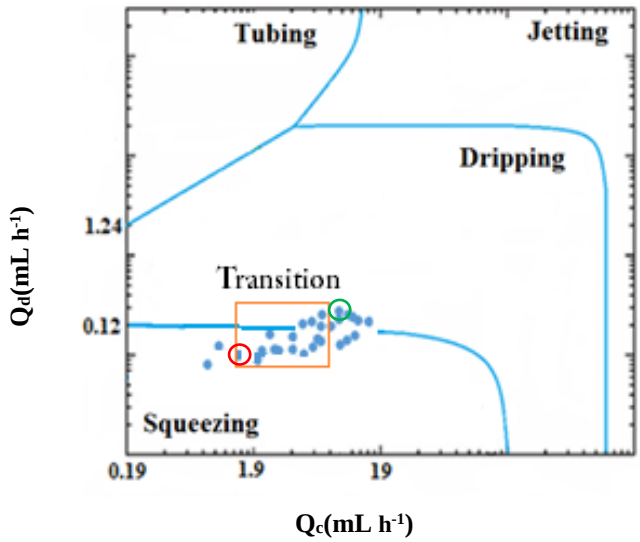

(a)

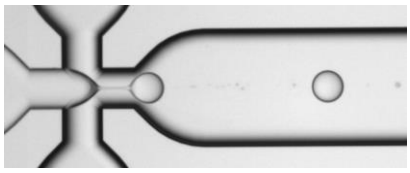

(i) Droplet formation at the bottom of the transition regime (red circle on Figure 4-a)

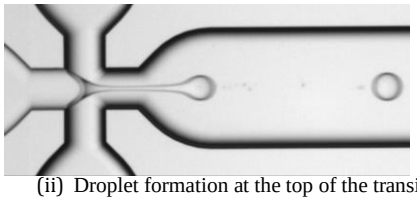

(ii) Droplet formation at the top of the transition regime (green circle on Figure 4-a)

(b)

Figure 4: (a) Flow patterns cartography of the different hydrodynamic regimes in the FF-junction depending on dispersed (Dodecane – [DMDBTDMA]= 1 M) and continuous phase ([HNO_3] = 4 M – [Eu(III)] = 10^{-2} M) flow rates. Blue points are experimental data. Transition regime is defined by Q_c range [1.9; 7.6 mL.h^{-1}] corresponding to Ca_c range [0.002; 0.008] established on the basis of [34, 37, 38]. (b) (i) squeezing-like droplet formation, (Q_c, Q_d) = (1.69 mL.h^{-1}, 0.08 mL.h^{-1}), (ii) dripping-like droplet formation, (Q_c, Q_d) = (10.08 mL.h^{-1}, 0.22 mL.h^{-1}).

3.2 Droplet size determination

Two relations allow to calculate the size of the formed droplets, the first in the transition regime between squeezing and dripping, and the second in the dripping regime.
Liu and Zhang [37] defined the drop diameter l_{drop} in the transition regime, as described by relation (3).

$$\frac{l_{drop}}{w_c} = (\tilde{\varepsilon} + \tilde{\alpha}\frac{Q_d}{Q_c})Ca_c^{\tilde{m}} \qquad (3)$$

With $\tilde{\varepsilon}, \tilde{\alpha}$ *and* $\tilde{m}$ fitting parameters linked to microchannel geometry.

For higher flow rates, droplet generation in the dripping regime is exclusively ruled by capillary effects. In 2008, Cubaud and Mason [34] proposed empirical equations for deriving the plot length as a function of the continuous phase capillary number and flow rate ratio. They determined a relation between the ratio $\phi = \frac{Q_d}{Q_c}$, Ca_c and l_{drop} (relation 4).

$$\frac{l_{drop}}{h} \approx \begin{cases} 2.2.10^{-4}\left(\frac{1}{1+\phi}Ca_c\right)^{-1} & if \ \frac{l_{drop}}{h} > 2.5 \\ 0.5\left(\frac{1}{1+\phi}Ca_c\right)^{-0.17} & if \ \frac{l_{drop}}{h} < 2.5 \end{cases} \qquad (4)$$

Where h is the eight of the microchannel.

The two studies used empirical relations constructed separately and obtained with different microchannel sizes in a FF-junction, and various chemical systems. Our objective is to validate these relations for our FF-junction and the chosen chemical system and to validate the continuity between the two models.

3.3 Experimental validation of the droplet size models

To validate empirical equations of the transition and dripping regimes, flow rates couples were chosen in both ranges (Figure 4). Each time, segmented flows were recorded and video sequences processed with the DMV software.

Using relations (3) and (4), fitted to our results as (5) and (6), we determined the droplets volume V_{plot} (for droplets considered as spherical) and frequencies $f = \frac{Q_d}{V_{plot}}$.

$$\frac{l_{plot}}{w_c} = 0.625\ (\tilde{\varepsilon} + \tilde{\alpha}\frac{Q_d}{Q_c})Ca_c^{\tilde{m}} \quad (5)$$

and

$$\frac{l_{drop}}{h} \approx \begin{cases} 1.375.10^{-4}\left(\frac{1}{1+\phi}Ca_c\right)^{-1} & if\ \frac{l_{drop}}{h} > 2.5 \\ 0.3125\left(\frac{1}{1+\phi}Ca_c\right)^{-0.17} & if\ \frac{l_{drop}}{h} < 2.5 \end{cases} \quad (6)$$

Fitting parameters varied only by a factor 1.6 from the original empirical relations from Liu and Zhang [37], and Cubaud and Mason [34]. When adjusted to our experiments, these relations proved to be accurate.

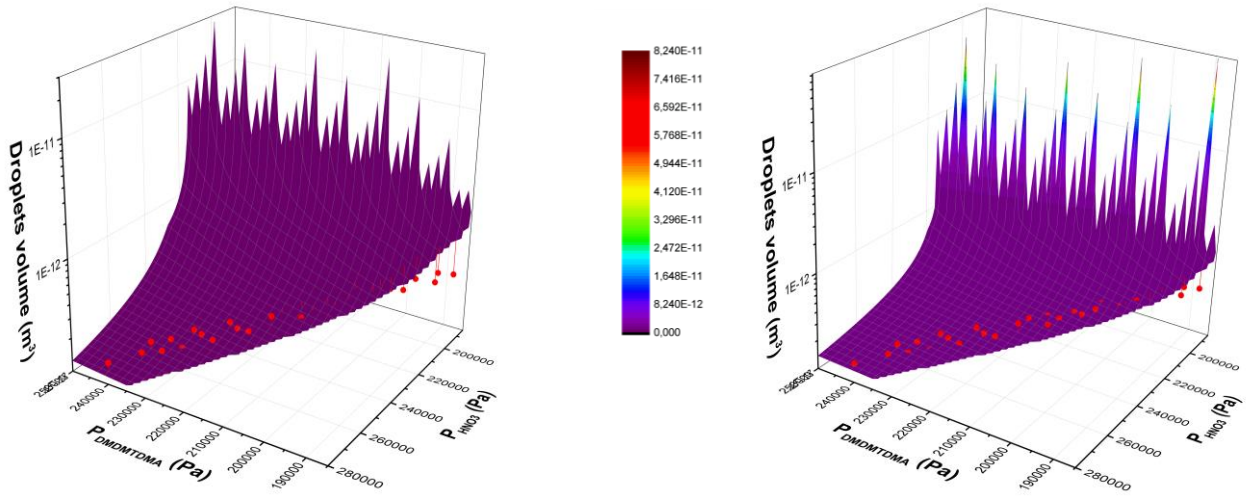

(a) **(b)**

Figure 5: Comparison between droplets volume calculated with the models and experimental values (red points) referring to the transition (a) and dripping (b) regimes.

Both empirical models showed a very good correlation with the experimental results for the determination of the droplet size (Figure 5), however showed a slight deviation for flow rates bordering the squeezing regime. Moreover, the two models can be used without discontinuity from the transition regime to the dripping one. This confirms the presence of capillary effects within the range of the transition regime, as Liu and Zhang predicted [37].

In a second time, we compared the droplets frequencies obtained with each empirical equation and the experimental values (Figures 6 and 7) obtained in the squeezing regime (Figure 4-b). Although the transition regime equation from Liu and Zhang predict slightly lower frequencies than Cubaud and Mason equation, these empirical equations are an extremely good fit for our experimental results.

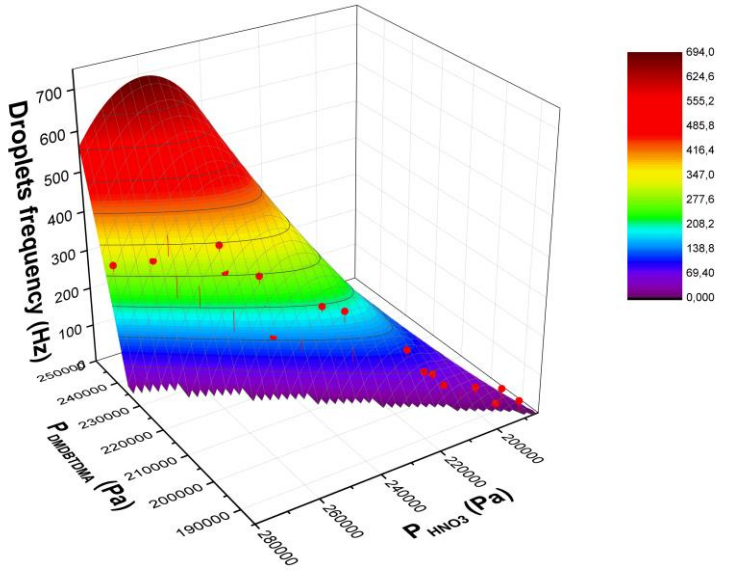

Figure 6: Comparison between the droplets frequency obtained experimentally (red points) or calculated with the equations of Liu and Zhang in the transition regime.

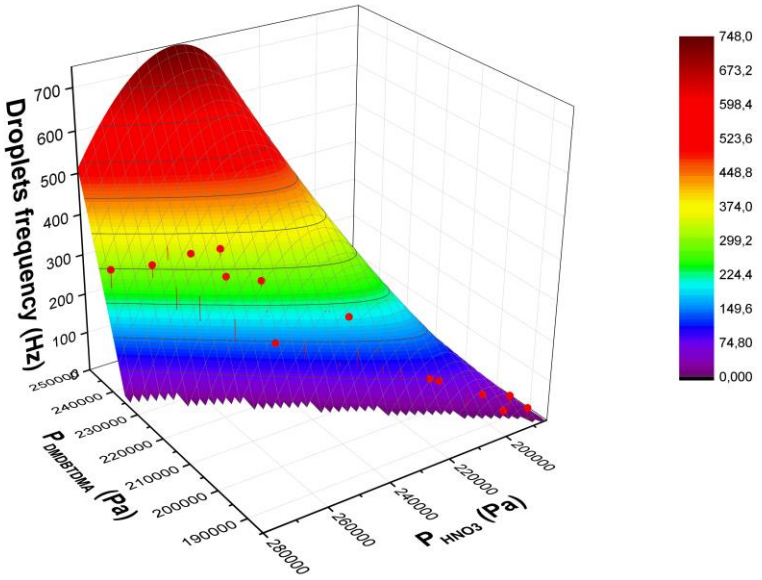

Figure 7: Comparison between the droplets frequency obtained experimentally (red points) or calculated with the equations of Cubaud and Mason in the dripping regime.

4 Conclusion

As a conclusion, these two validated models can be used in order to predict the droplet population characteristics (i.e. volumes, frequencies, spacing) for given flow rates within the transition regime. Now there is a validated tool to predict and calibrate the size of the droplets (related to flow rates and viscosities) involved in the calculation of the specific interfacial area, we should be able to optimize mass transfer in FF-junctions.

Greetings

The authors thank Amar S. Basu, from Electrical and Computer Engineering and Biomedical Engineering Departments, Wayne State University, 5050 Anthony Wayne Drive, Detroit MI 48202, USA, for the Droplet Morphometry and Velocimetry software he developed.

References

[1] G. Hellé et al., Toward numerical prototyping of labs-on-chip: modeling for liquid–liquid microfluidic devices for radionuclide extraction, Microfluidics and Nanofluidics 19(5) (2015) 1245-1257

[2] G. Hellé, C. Mariet, G. Cote, Liquid–liquid microflow patterns and mass transfer of radionuclides in the systems Eu(III)/HNO_3/DMDBTDMA and U(VI)/HCl/Aliquat® 336, Microfluidics and Nanofluidics 17(6) (2014) 1113-1128

[3] R.O.A. Rahman, H.A. Ibrahium, Y.-T. Hung, Liquid radioactive wastes treatment: A review, Water 3(4) (2011) 551-565

[4] G. Janssens-Maenhout, G., The benefits of applying microsystems in radiochemistry, Nanotechnology Perceptions 3 (2007) 183-192

[5] G. Janssens-Maenhout, J. Buyst, P. Peerani, Reducing the radioactive doses of liquid samples taken from reprocessing plant vessels by volume reduction, Nuclear Engineering and Design 237(8) (2007) 880-886

[6] M. Tokeshi, T. Minagawa, T. Kitamori, Integration of a microextraction system on a glass chip: Ion-pair solvent extraction of Fe(II) with 4,7-Diphenyl-1,10-phenanthrolinedisulfonic acid and Tri-n-octylmethylammonium chloride, Analytical Chemistry 72 (2000) 1711-1714

[7] L. Shui, J.C. Eijkel, A. van den Berg, Multiphase flow in microfluidic systems --control and applications of droplets and interfaces, Adv Colloid Interface Sci 2007. 133(1) (2007) 35-49

[8] D. Mark et al., Microfluidic lab-on-a-chip platforms: requirements, characteristics and applications, Chemical Society Review 39(3) (2010) 1153-1182

[9] A.-L. Dessimoz, et al. Liquid–liquid two-phase flow patterns and mass transfer characteristics in rectangular glass microreactors, Chemical Engineering Science, 2008. 63(16): p. 4035-4044.

[10] Cote, G., Extraction liquide-liquide - Présentation générale, Techniques de l'ingénieur, J2760, 1998.

[11] G.F. Christopher, S.L. Anna, Microfluidic methods for generating continuous droplet streams, Journal of Physics D: Applied Physics 40(19) (2007) R319-R336

[12] T. Maruyama et al., Liquid membrane operations in a microfluidic device for selective separation of metal ions, Analytical Chemistry 76: (2004) 4495-4500

[13] G. Hellé, G., Microsystèmes séparatifs pour l'extraction liquide-liquide des radioéléments dans les protocoles d'analyse, Thèse Université Paris VI, 2014.

[14] J.R. Burns and C. Ramshaw, The intensification of rapid reactions in multiphase systems using slug flow in capillaries, Lab Chip 1(1) (2001) 10-15

[15] A. Ufer et al., Liquid/liquid slug flow capillary microreactor, Chemical Engineering & Technology 34(3) (2011) 353-360

[16] C. King, E. Walsh, R. Grimes, PIV measurements of flow within plugs in a microchannel, Microfluidics and Nanofluidics 3(4) (2007) 463-472

[17] M. Wegener, N. Paul, M. Kraume, Fluid dynamics and mass transfer at single droplets in liquid/liquid systems, International Journal of Heat and Mass Transfer 71(2014) 475-495

[18] D. Tsaoulidis, P. Angeli, Effect of channel size on mass transfer during liquid–liquid plug flow in small scale extractors. Chemical Engineering Journal, 262 (2015) 785-793

[19] H. Song, H., J.D. Tice, and R.F. Ismagilov, A microfluidic system for controlling reaction networks in time, Angewandte Chemie International Edition English 42(7) (2003) 767-772
[20] D. Tsaoulidis et al., Dioxouranium (VI) extraction in microchannels using ionic liquids, Chemical Engineering Journal 227 (2013) 151-157
[21] A. Aota et al., Countercurrent laminar microflow for highly efficient solvent extraction, Angewandte Chemie International Edition English 46(6) (2007) 878-880
[22] M.N. Kashid, L. Kiwi-Minsker, Microstructured reactors for multiphase reactions: State of the art, Industrial & Engineering Chemistry Research 48 (2009) 6465-6485
[23] N. Assmann, A. Ładosz, and P. Rudolf von Rohr, Continuous micro liquid-liquid extraction, Chemical Engineering & Technology 36(6) (2013) 921-936
[24] Fries, D.M., T. Voitl, and P.R. von Rohr, Liquid Extraction of Vanillin in Rectangular Microreactors, Chemical Engineering & Technology 31(8) (2008) 1182-1187
[25] B. Ahmed, D. Barrow, T. Wirth, Enhancement of reaction rates by segmented fluid flow in capillary scale reactors, Advanced Synthesis & Catalysis 348(9) (2006) 1043-1048
[26] M. Weigl et al., Kinetics of lanthanide/actinide co-extraction with N,N′-Dimethyl-N,N′-Dibutyltetradecylmalonic Diamide (DMDBTDMA). Solvent Extraction and Ion Exchange 19(2) (2001) 215-229
[27] A. M. Ganan-Calvo, J.M. Gordillo, Perfectly monodisperse microbubbling by capillary flow focusing. Physical Review Letters 87(27 Pt 1) (2001) 274501
[28] S.L. Anna, N. Bontoux, and H.A. Stone, Formation of dispersions using "flow focusing" in microchannels. Applied Physics Letters 82(3) (2003) 364-366
[29] P. Garstecki, H.A. Stone, G.M. Whitesides, Mechanism for flow-rate controlled breakup in confined geometries: a route to monodisperse emulsions, Physical Review Letters 94(16) (2005) 164501
[30] S.L. Anna, H.C. Mayer, Microscale tip streaming in a microfluidic flow focusing device, Physics of Fluids 18(12) (2006) 121512
[31] S.J. Ashcroft, D.R. Booker, J.C.R. Turner, Density measurement by oscillating tube, Journal of Chemical Society 86(1) (1990) 145-149
[32] A.S. Basu, Droplet morphometry and velocimetry (DMV): a video processing software for time-resolved, label-free tracking of droplet parameters, Lab Chip 13(10) (2013) 1892-1901
[33] T. Ward et al., Microfluidic flow focusing: drop size and scaling in pressure versus flow-rate-driven pumping, Electrophoresis 26(19) (2005) 3716-3724
[34] T. Cubaud, T.G. Mason, Capillary threads and viscous droplets in square microchannels, Physics of Fluids 20(5) (2008) 053302
[35] A.R. Abate et al., Impact of inlet channel geometry on microfluidic drop formation, Physical review. E, Statistical, nonlinear, and soft matter physics American Physical Society 80(2 Pt 2) (2009) 026310
[36] M. Seo et al., Microfluidic consecutive flow-focusing droplet generators, Soft Matter 3(8) (2007) 986
[37] H. Liu, Y. Zhang, Droplet formation in microfluidic cross-junctions, Physics of Fluids 23(8) (2011) 082101
[38] J.K. Nunes, S. S. Tsai, J. Wan, H. A. Stone, Dripping and jetting in microfluidic multiphase flows applied to particle and fiber synthesis, Journal of Physics D: Applied Physics, 46(11) (2013) 114002